Cross-stream migration and coalescence of droplets in a microchannel co-flow using magnetophoresis

Cite as: Phys. Fluids **31**, 112003 (2019); https://doi.org/10.1063/1.5123533
Submitted: 07 August 2019 . Accepted: 28 October 2019 . Published Online: 13 November 2019

U. Banerjee, C. Mandal, S. K. Jain, and A. K. Sen

Cross-stream migration and coalescence of droplets in a microchannel co-flow using magnetophoresis

Cite as: Phys. Fluids 31, 112003 (2019); doi: 10.1063/1.5123533
Submitted: 7 August 2019 • Accepted: 28 October 2019 •
Published Online: 13 November 2019

U. Banerjee, C. Mandal, S. K. Jain, and A. K. Sen[a)]

AFFILIATIONS

Department of Mechanical Engineering, Indian Institute of Technology Madras, Chennai 600036, India

[a)]Author to whom correspondence should be addressed: ashis@iitm.ac.in

ABSTRACT

Manipulation of aqueous droplets in microchannels has great significance in various emerging applications such as biological and chemical assays. Magnetic-field based droplet manipulation that offers unique advantages is consequently gaining attention. However, the physics of magnetic field-driven cross-stream migration and the coalescence of aqueous droplets with an aqueous stream are not well understood. Here, we unravel the mechanism of cross-stream migration and the coalescence of aqueous droplets flowing in an oil based ferrofluid with a coflowing aqueous stream in the presence of a magnetic field. Our study reveals that the migration phenomenon is governed by the advection (τ_a) and magnetophoretic (τ_m) time scales. Experimental data show that the dimensionless equilibrium cross-stream migration distance δ^* and the length $L_\delta{}^*$ required to attain equilibrium cross-stream migration depend on the Strouhal number, $St = (\tau_a/\tau_m)$, as $\delta^* = 1.1\ St^{0.33}$ and $L_\delta{}^* = 5.3\ St^{-0.50}$, respectively. We find that the droplet-stream coalescence phenomenon is underpinned by the ratio of the sum of magnetophoretic (τ_m) and film-drainage time scales (τ_{fd}) and the advection time scale (τ_a), expressed in terms of the Strouhal number (St) and the film-drainage Reynolds number (Re_{fd}) as $\xi = (\tau_m + \tau_{fd})/\tau_a = (St^{-1} + Re_{fd})$. Irrespective of the flow rates of the coflowing streams, droplet size, and magnetic field, our study shows that droplet-stream coalescence is achieved for $\xi \leq 50$ and ferrofluid stream width ratio $w^* < 0.7$. We utilize the phenomenon and demonstrated the extraction of microparticles and HeLa cells from aqueous droplets to an aqueous stream.

I. INTRODUCTION

Manipulation of micro/nanodroplets has received significant attention from the research community owing to their smaller length scale and lower volume, and the community has found important applications in biological[1] and chemical[2] assays. Depending on the mode of operation, the area of droplet microfluidics can be broadly categorized into digital and continuous microfluidics. Digital microfluidics enables transportation,[3] merging,[4] and splitting[5] of discrete droplets on engineered surfaces. On the other hand, continuous microfluidics deals with the manipulation of a large number of continuous droplets inside microchannels.[6,7] Based on the actuation mechanism, droplet microfluidics can be further classified in terms of active and passive techniques. In passive techniques, droplet manipulation is achieved using the hydrodynamic forces such as noninertial lift,[7] inertial lift,[8] dean force,[9] and Marangoni convection.[10,11] On the contrary, active techniques utilize external stimuli such as optical,[12] electrical,[13] and magnetic[14,15] fields for the droplet manipulation.

Among the various active techniques available for droplet manipulation, magnetic field based techniques offer distinctive advantages such as contactless actuation, lower heat generation, and biocompatibility. This technique is versatile and enables the manipulation[16] of both magnetic and nonmagnetic objects. Depending on the nature of the objects to be manipulated, magnetic manipulation techniques can be further classified into positive and negative magnetophoresis. Positive magnetophoresis deals with the manipulation of magnetic objects in the vicinity of a magnetic field which is used for manipulating magnetically tagged cells,[17] magnetic beads,[18] and ferrofluid droplets.[19,20] On the other hand, manipulation of

diamagnetic objects such as aqueous droplets comes under negative magnetophoresis.[21,22]

Manipulation and size based sorting of magnetic droplets, i.e., aqueous droplets loaded with magnetic nanoparticles, under a magnetic field has been demonstrated.[23] Magnetophoretic sorting of droplets containing magnetic nanoparticles and microalgal cells has been reported in which the nanoparticle concentration, droplet size, velocity, and magnetic strength were tuned to achieve improved performance.[24] Magnetic droplets can be either droplets loaded with magnetic nanoparticles (size ≥10 nm) or ferrofluids that comprise colloidal suspensions of ferromagnetic particles (particle size ~10 nm) suspended in oil or water.[25] Recently, manipulation of ferrofluid droplets across the interface between two coflowing immiscible liquids has been demonstrated,[26] wherein the interplay between the magnetic force, interfacial tension, and noninertial lift force governed the interfacial migration phenomenon. While use of positive magnetophoresis for manipulation of magnetic objects has been widely studied, limited studies are available on negative magnetophoresis.

Focusing of nonmagnetic particles[27,28] and biological cells[29] has extensive applications in microfluidics. There exist several passive and active techniques such as acoustics,[30] magnetic,[31] and inertial[32,33] techniques that demonstrate focusing of nonmagnetic particles inside microchannels. The focusing of microparticles inside a microchannel using two permanent magnets with their axis of magnetization in a direction normal to the channel length has been studied.[34] The principle of focusing lies in the fact that nonmagnetic particles experience a magnetic buoyancy force in the presence of a nonuniform magnetic field, which pushes them toward the lowest magnetic field region located at the center of the channel. Trapping of aqueous droplets present in an oil based ferrofluid into microwells located on one side of a microchannel has been investigated.[35] A recent study[36] dealt with size based separation of diamagnetic particles in an aqueous ferrofluid stream coflowing with an aqueous stream in a microchannel in the presence of a microscale magnet. The larger diamagnetic particles suspended in the aqueous ferrofluid migrate toward the water-ferrofluid interface due to negative magnetophoresis, thus facilitating size based separation of particles. A review of the literature indicates that although a few attempts have been made toward utilizing negative magnetophoresis for trapping of droplets and sorting of particles in microchannels, the physics of cross-stream migration of aqueous droplets in an oil based ferrofluid due to the negative magnetophoretic force has not been studied, which we address in the present work.

As discussed, droplets have tremendous applications in microfluidics. The motion of droplets can be manipulated to achieve droplet-droplet and droplet-stream coalescence that has important applications in microfluidics. Passive coalescence of droplets is challenging owing to a longer film drainage time compared to the residence time.[37,38] External fields such as electric[39] and magnetic[40] fields have been used for the coalescence of droplets. Recently, the coalescence of aqueous droplets in an oil stream with a coflowing aqueous stream has been reported.[13] It was observed that use of a high electric field can degrade the electrodes and adversely affect the viability of biological contents of the droplets. Such problems can be avoided by using a magnetic field, which is known to be contactless and biocompatible. However, the mechanism of the magnetic field based coalescence of droplets with liquid stream has not been investigated yet.

Here, we study the physics of cross-stream migration and the coalescence of aqueous droplets in an oil based ferrofluid coflowing with an aqueous stream in the presence of a magnetic field. We find that the droplet relocation phenomenon depends on the advection time scale (τ_a) and magnetic time scale (τ_m), and the magnitude of cross-stream migration depends on the ratio of these two time scales. Our study shows that the magnetic field-driven coalescence of aqueous droplets with an aqueous stream depends on the ratio of the sum of magnetic time scale (τ_m) and thin-film drainage time scale (τ_{fd}) to the advection time scale (τ_a). We utilize the proposed magnetocoalescence phenomenon to demonstrate the extraction of microparticles and HeLa cells from aqueous droplets into an aqueous stream.

II. THEORETICAL

Figures 1(a) and 1(b), respectively, depict the magnetic field-driven cross-stream migration and the coalescence of aqueous droplets in an oil based ferrofluid with a coflowing aqueous stream. We first discuss the various forces that contribute toward cross-stream migration of droplets in the presence of a magnetic field. At low Reynolds numbers ($Re < 1$), depending on the size, deformability, shear rate, viscosity ratio, and orientation and the lateral position with respect to the channel wall, droplets will experience a lift force known as noninertial or deformability induced lift force F_l,[7,26] which is given as

$$F_l = \frac{C_l \mu_f \dot{\gamma} d^3}{8y}, \tag{1}$$

where $\dot{\gamma}$ is the shear rate, d is the diameter of the aqueous droplet, μ_f is continuous phase (ferrofluid) viscosity that is assumed to be independent of the magnetic field and the shear rate, based on the comparison of hydrodynamic stress and the magnetic stress[41] as $\frac{\dot{\gamma}\mu_0}{MH} < 10^{-6}$, y is lateral position from the channel wall, and C_l is the lift coefficient that depends on the droplet size, orientation, and viscosity ratio. Owing to the noninertial lift force F_l, the droplets would tend to migrate toward the zone of minimum shear, which is located at the centerline of the channel in a Poiseuille flow such as the present case.

Diamagnetic objects, such as aqueous (water) droplets, present inside a magnetic or paramagnetic medium (ferrofluid), when exposed to a nonuniform magnetic field, experience a force termed as the negative magnetophoretic force (F_{nm}), which is given as[35]

$$F_{nm} = \frac{V_d \Delta\chi}{\mu_0}(B \cdot \nabla)B, \tag{2}$$

where V_d is the volume of the aqueous droplet, $\Delta\chi = \chi_d - \chi_f$ is the difference in the magnetic susceptibility of the droplet and the ferrofluid medium, in the present study $\chi_d \sim -10^{-5}$ and $\chi_f \sim 0.05$ to 6.79, which gives $\Delta\chi \sim 0.05$ to 6.79, B is the magnetic flux density (T) ∇B is the flux gradient (Tm^{-1}), and μ_0 is the permeability of vacuum ($4\pi \times 10^{-7}$ H/m).

Here, the flow rate of the ferrofluid stream Q_f varies in the range 5–40 μl/min for which the average shear rate $\dot{\gamma}$ varies between 9.25 s^{-1} and 74.03 s^{-1} and $\mu_f \approx 10^{-3}$ and $C_L \approx 0.1$. For an

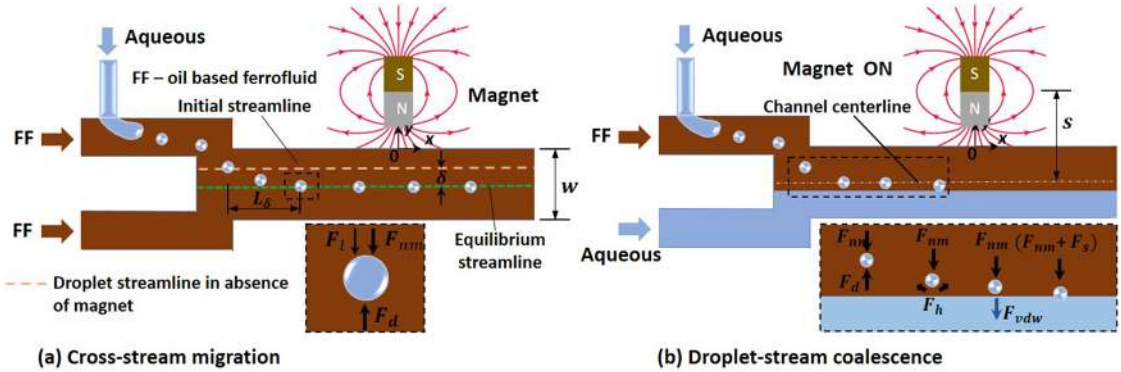

FIG. 1. Schematic diagram of the magnetic field based (a) cross-stream migration of droplets—in the absence of magnetic field, droplets follow their initial streamlines. In the presence of the magnetic field, the droplets undergo cross-stream migration, equilibrium cross-stream migration δ, and the distance required L_δ are shown, (b) the coalescence of droplets—droplets are pushed toward the coflow interface and coalescence of the droplets with the aqueous stream is achieved; the various forces acting on a droplet as it proceeds from its initial streamline toward the interface for coalescence are shown.

aqueous droplet of 80 μm diameter located at a distance of 50 μm from the side wall, the maximum value of the lift force is estimated to be $F_l \sim 10^{-12}$ N, which is much smaller compared to the negative magnetphoretic force, which is in the range $\sim 10^{-9}$ N to 10^{-6} N, depending on the location of the magnet. Thus, the effect of the noninertial lift force on the cross-stream migration can be safely neglected.

When the aqueous droplet moves laterally due to the negative magnetophoretic force, its motion will be opposed by the viscous drag. Considering the Reynolds number to be small ($Re < 1$), the drag force acting on the droplet is given as

$$F_d = 3\pi\mu_f d U_l, \tag{3}$$

where U_l is the average lateral velocity of the droplet along the y-direction. The average lateral velocity is used to estimate the magnetophoretic time scale. The droplet will migrate over a lateral distance δ, depending on the ratio of the magnetophoretic and advection time scales, as discussed later.

The coalescence of an aqueous droplet in an oil based ferrofluid stream with a coflowing aqueous stream occurs in four consecutive steps [Fig. 1(b)]. First, the negative magnetophoretic force pushes the droplet in the lateral direction toward the interface, which leads to the formation of a thin film between the droplet and the interface. Second, when the droplet approaches the interface, continuous drainage of the oil film between the droplet-oil and the oil-aqueous interfaces takes place, which gives rise to a hydrodynamic force[42] given by

$$F_h = -\left(\frac{3\pi\mu_f d^4}{2\beta h^3}\right)\left(\frac{dh}{dt}\right), \tag{4}$$

where h is the dynamic thickness of the thin film and $\beta = 4$ for a moving droplet.[42] From scaling, we estimated that the magnitude of $F_h \sim 10^{-9}$ N, which is of the same order of magnitude as F_{nm}. Third, as the droplet moves further closer to the interface, at a much thinner interface thickness (~25 to 50 nm), the magnetic force needs to overcome the molecular forces originating from disjoining pressure. There are three key components of disjoining pressure: the van der Waals force, steric forces, and electrostatic double layer (EDL) force. The steric and EDL forces are repulsive in nature and are realized when surfactant molecules are present in the system.[43] Here, due to the presence of oleic acid (surfactant) in the oil based ferrofluid, in addition to the van der Waals force, steric and EDL forces will be relevant. From scaling, we find that the steric force ($\sim E_{r,max}/\varepsilon$), where $E_{r,max}$ is the maximum potential energy due to steric repulsion (~50 kT) and ε (~10 nm) is the length scale and scales as $\sim 10^{-11}$ N, k—Boltzmann constant, and T—absolute temperature (K). EDL forces appear due to the formation of an electric double layer at the charged interfaces and hence negligible as compared to the van der Waals force ($\sim 10^{-9}$ N).

If the oil (ferrofluid) film becomes sufficiently thin and approaches a critical thin film thickness, the effects of van der Waals force,[13,44] which acts toward the aqueous stream (since it is attractive in nature), can rupture the thin film of ferrofluid leading to instant coalescence of the aqueous droplet with the aqueous stream. This critical film thickness can be expressed as[45] $h_c = 0.267\left(a_f A_h^2/6\pi\sigma_i\Delta p\right)^{\frac{1}{7}}$, where a_f is the area of the film, A_h is the Hamaker constant[46] ($\sim 10^{-19}$ J), σ_i is the interfacial tension between ferrofluid and aqueous streams, and Δp is the excess pressure in the film due to the negative magnetophoretic force acting on the aqueous droplet. By performing an order of magnitude analysis for a droplet of 30 μm diameter, we found that $h_c \approx 33$ nm. From the literature, the critical film thickness value is <50 nm for emulsion films.[45] Therefore, we take that the critical thin film thickness in our case will be of the order of 29 nm–35 nm. The van der Waals force F_{vdw} scales as $\sim A_H a/3\pi h^2$, where A_H is the Hamaker constant and h is the thickness of the thin film.[47] For 30 nm of film thickness, the van der Waals force will be in the order of $\sim 10^{-9}$ N, which is of the same order of magnitude as the negative magnetophoretic force. As the film thickness reduces further, the van der Waals force dominates over the negative magnetophoretic force which leads to the rupture of the ferrofluid film and instant coalescence occurs. Finally, once the thin film is ruptured, the force due

to Laplace pressure F_s (i.e., excess pressure inside the drop) facilitates movement of the liquid inside the droplets into the aqueous stream.

III. EXPERIMENTAL

An SU8 photoresist master is prepared using photolithography, and the microchannel device is fabricated in polydimethylsiloxane (PDMS) by the following standard soft lithography procedure elaborated elsewhere.[48] In the fabricated device, the expanded channel section has a width of 300 μm and a depth of 100 μm. An oil based ferrofluid (EMG 901, Ferrotec, Singapore) of density 1430 kg/m^3 and viscosity 8 mPa s was diluted using kerosene as the diluent with magnetic nanoparticles (magnetite) at 2% v/v and was used as the carrier phase for the droplets. The viscosity of the diluted ferrofluid was found to be ≈2 mPa s. Deionized water (resistivity of 18.2 MΩ cm, Millipore) is used as the droplet phase. Kerosene is used to dilute the oil based ferrofluid and vary the MNP concentration. Two neodymium iron boron (NdFeB, N52) permanent magnets (M1 and M2) of size ($2l = 2b = 2h = 4.7625$ mm) and ($2l = 2b = 2h = 12.7$ mm) and remanent flux density 14.8 T (K&J Magnetics, Inc., USA) are used to provide the nonuniform magnetic field in the case of droplet relocation and coalescence, respectively. The distance between the center of the magnet, and the centerline of the microchannel is maintained to be in the range 3–9 mm. An aqueous suspension of polystyrene beads (Sigma Aldrich, India) of size 10 μm at a volume fraction of 0.3% is used in the bead extraction experiments. In order to avoid the settling of the microbeads, the density of the aqueous phase is matched with that of polystyrene beads by adding 22.5% wt/wt glycerol (Sigma Aldrich, India) in water. To prevent agglomeration and inhibit adhesion of microbeads with the microchannel walls, Tween 80 (Sigma Aldrich, India) 0.5% v/v is added to DI water. To demonstrate cell extraction experiments, the HeLa (cervical cancer) cell line was obtained from the National Centre for Cell Science (NCCS) (Pune, India) and grown according to the protocol reported elsewhere.[49] The continuous and discrete phases are infused using a high-performance syringe pump (neMESYS Pump, Cetoni, Germany). The fluidic connection between the microchannel device and the syringe pumps is established using PTFE tubing (Sigma Aldrich, India). The droplet motion is captured using an inverted microscope (Olympus) coupled with a high-speed camera (FASTCAM SA4 model, Photron USA, Inc.) operating at 500 fps and interfaced with a Personal Computer (PC) via Photron Fastcam Viewer software. A photograph of the device (with the magnet in place) and a schematic of the experimental setup are presented in the supplementary material (see Fig. S1).

IV. RESULTS AND DISCUSSION

First, cross-stream migration of aqueous droplets flowing in a stream of oil based ferrofluid and exposed to a magnetic field is presented and discussed. The dependence of the equilibrium cross-stream migration distance and the length required to attain this equilibrium position on relevant dimensionless parameters is studied. Next, the coalescence of aqueous droplets with a coflowing aqueous stream is illustrated and coalescence and noncoalescence regimes are characterized. Finally, the extraction of microparticles and HeLa cells from aqueous droplets into a coflowing aqueous stream is demonstrated.

A. Cross-stream migration of droplets

In our study on cross-stream migration of aqueous droplets in the oil based ferrofluid [Fig. 1(a)], the device consists of two regions: the droplet generator and magnetic field regions (in an expanded channel). The droplet generator is used for producing aqueous droplets in the oil based ferrofluid. By varying the discrete phase (aqueous) flow rate in the range 0.5–4 μl/min and the continuous phase (ferrofluid) flow rate in the range 5–40 μl/min, droplets of diameters ranging from 20 to 120 μm were generated at frequencies ranging from 4 to 20 Hz. The distance between the droplets was measured to be in the range 100–500 μm.

The droplets entering the magnetic field region are subjected to the negative magnetophoretic force and thus exhibit cross-stream migration that mainly depends on three parameters—the droplet size (d), the location of the incoming droplet with respect to the magnetic field, and the flow rate of the ferrofluid (Q_f). Experimental images of cross-stream migration of droplets at different conditions are presented in Fig. 2. The effect of the droplet location with respect to the magnet is expressed in terms of B and ∇B, which are obtained from MATLAB (see Sec. S.2 in the supplementary material). It is observed that, over a fixed length of the channel, a larger equilibrium cross-stream migration distance δ^* (defined as $\delta^* = \delta/w$) can be obtained by using a stronger magnetic field [Figs. 2(a-i) and 2(a-ii)] and for a larger droplet size [Figs. 2(a-iii) and 2(a-iv)], whereas a higher ferrofluid flow rate gives rise to a smaller cross-stream migration distance [Figs. 2(a-v) and 2(a-vi)]. In Figs. 2(a-i) and 2(a-ii), with $d = 55$ μm and $Q_f = 20$ μl/min, by increasing the magnetic field from $(B \cdot \nabla B)$ from 0.06 T^2/m to 0.51 T^2/m, δ^* increases from 0.10 to 0.40. In Figs. 2(a-iii) and 2(a-iv), with $(B \cdot \nabla B) = 1.25$ T^2/m and $Q_f = 20$ μl/min, if the droplet size increases from 28 to 45 μm, δ^* increases from 0.20 to 0.32. Similarly, in Figs. 2(a-v) and 2(a-vi), with $d = 55$ μm and $(B \cdot \nabla B) = 0.51$ T^2/m, if the flow rate of the ferrofluid is increased from 10 μl/min to 15 μl/min, δ^* reduces from 0.41 to 0.19.

The parameter $(B \cdot \nabla B)$ can be varied by changing the strength and location of the magnet. The effect of the position of the magnet with respect to the incoming droplets on the droplet trajectory is depicted in Fig. 2(b) (Multimedia view). In the absence of a magnetic field, the droplet faithfully follows its original streamline and does not exhibit any considerable cross-stream migration. Depending on the axial position of the magnet along the channel and the proximity of the magnet to the channel walls, different droplet trajectories are observed. We observe that if the position of the magnet is shifted in the axial direction, it simply alters the trajectory of cross-stream migration. In Fig. 2(b) (Multimedia view), the magnet is axially shifted from $\Delta x = 0$, $\Delta y = 0$ to $\Delta x = -2.4$ mm, $\Delta y = 0$ due to which the location of migration shifts by the same amount ($\Delta x = -2.4$ mm). However, the magnitude of the equilibrium cross-stream migration distance δ as well as the distance L_δ remains the same. On the other hand, the spacing between the magnet and channel wall affects the droplet trajectory and the migration distance δ. A smaller gap ($\Delta x = 0$, $\Delta y = 0$) leads to a higher migration distance δ as compared to a larger gap ($\Delta x = 0$, $\Delta y = 4$ mm), which is attributed to a higher magnetic field in the former case, as shown

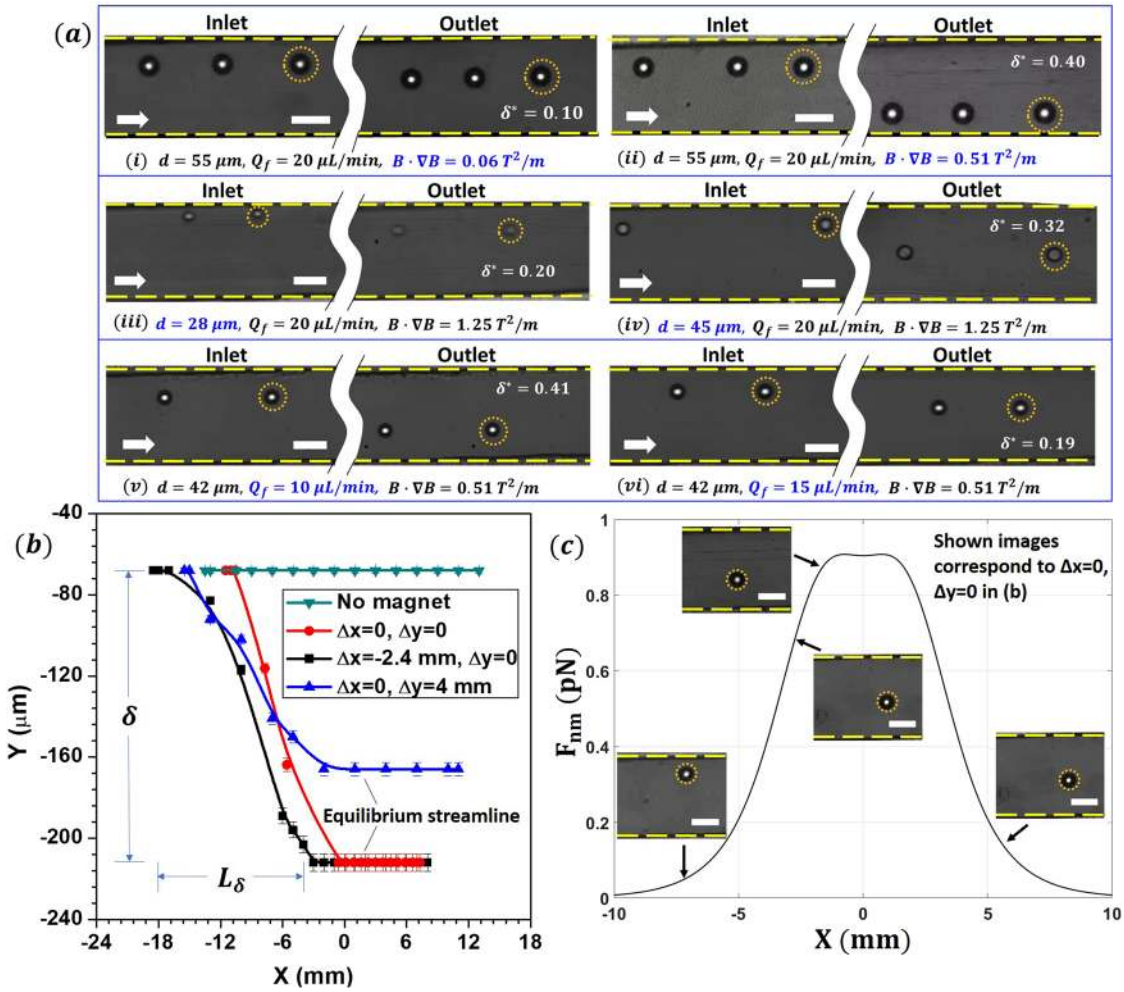

FIG. 2. (a) Experimental images of cross-stream migration of droplets showing the effect of (i and ii) the magnetic field, d = 55 μm, Q_f = 20 μl/min, and $(B \cdot \nabla B)$ = 0.06–0.51 T^2/m, (iii and iv) the droplet diameter, d = 28–45 μm, Q_f = 20 μl/min, and $(B \cdot \nabla B)$ = 1.25 T^2/m, and (v and vi) flow rate d = 55 μm, Q_f = 10–15 μl/min, and $(B \cdot \nabla B)$ = 0.51 T^2/m. (b) The effect of the position of the magnet with respect to the incoming droplets on the droplet trajectory, axial direction (Δx = −2.4 mm, Δy = 0), and lateral direction (Δx = 0, Δy = 4 mm), and droplet trajectory in the absence of the magnet is also shown. (c) Variation of the magnetic force (across the channel width) along the flow direction; images of the cross-stream migration of droplets are shown in the inset, magnet location s = 0.6 cm. Multimedia view: (b) https://doi.org/10.1063/1.5123533.1

in Fig. 2(b) (Multimedia view). However, the distance L_δ can change or remains the same. We also observed that a lower flow rate and a higher droplet size have a similar effect to that due to a reduced gap between the magnet and the channel (see Sec. S.3 in the supplementary material). We observe that irrespective of the operating conditions, the equilibrium migration streamline is attained at an axial location coinciding with the upstream edge of the magnet, where the magnetic force is the highest [see Fig. 2(c)]. Here, the magnetic force is estimated from MATLAB (see Sec. S.2 in the supplementary material).

The combined effect of the above governing parameters is represented by the transient Strouhal number St,[30,50] which is the ratio of the advection time scale τ_a and the magnetic time scale τ_m, i.e., $St = (\tau_a/\tau_m)$—a smaller time scale correspondingly indicates a stronger effect. In the present case, the advection time scale and the magnetic time scale control the axial and lateral migration of droplets, respectively. The advection time scale can be expressed as follows:

$$\tau_a = \frac{w}{\bar{U}_f} = \frac{w^2 h}{Q_f}. \tag{5}$$

Here, w and h are the channel width and height, respectively, and $\bar{U}_f$ is the average velocity of the ferrofluid inside the channel, which is given as $\bar{U}_f = \left(Q_f/wh\right)$. The magnetic time scale is expressed as follows:

$$\tau_m = \left(\frac{w}{U_l}\right) = \frac{18}{\pi}\left(\frac{w\mu_0\mu_f}{\Delta\chi(B \cdot \nabla B)d^2}\right). \tag{6}$$

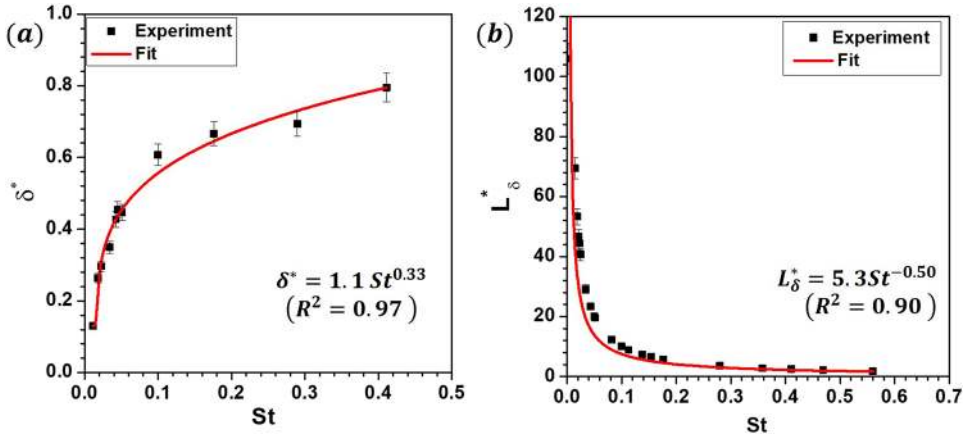

FIG. 3. (a) The variation of the magnitude of dimensionless equilibrium cross-stream migration distance $\delta^* = (\delta/w)$ with the Strouhal number $St = (\tau_a/\tau_m)$. (b) The variation of the dimensionless length required for attaining the equilibrium location $L_\delta^* = (L_\delta/w)$ with the Strouhal number St.

Here, U_l is found by equating the drag force [Eq. (3)] with the magnetophoretic force [Eq. (2)].

The variation of the magnitude of the dimensionless equilibrium cross-stream migration distance $\delta^* = (\delta/w)$ with the Strouhal number St is presented in Fig. 3(a), which shows that the cross-stream migration distance δ increases with an increase in the St. Fitting of the experimental data shows that δ^* and St are correlated as follows: $\delta^* = 1.1\ St^{0.33}$ (with $R^2 = 0.97$). Similarly, the variation of the dimensionless length required for attaining the equilibrium location $L_\delta^* = (L_\delta/w)$ with the Strouhal number St is studied. We found that L_δ^* decreases with an increase in the Strouhal number St, as shown in Fig. 3(b). From the experimental data, L_δ^* and St are correlated as follows: $L_\delta^* = 5.3\ St^{-0.50}$ (with $R^2 = 0.90$). Since St represents the ratio of advection to magnetophoretic time scales, $St \gg 1$ implies that the magnetophoretic effect is more dominant as compared to the advection effect, and similarly, $St \ll 1$ indicates that the advection effect is more dominant compared to the magnetophoretic effect. When $St \ll 1$, δ^* tends to zero, which indicates negligible cross-stream migration, and consequently, L_δ^* approaches to ∞. On the other hand, when $St \ll 1$, δ^* tends to be very high, and in that case, L_δ^* tends to zero. When $St \approx 1$, δ^* approaches 1, i.e., the cross-stream migration distance δ becomes equal to the width of the channel and $L_\delta^* \approx 5$.

B. Forces and time scales governing magnetocoalescence

Here, we discuss the cross-stream migration of aqueous droplets toward the interface between the ferrofluid and coflowing aqueous streams, and the subsequent coalescence with the aqueous stream. In the coalescence study [see Fig. 1(b)], the device consists of two regions: the droplet generator and magnetic field regions with coflowing ferrofluid and aqueous streams. A stable interface between the ferrofluid and the aqueous stream is established by varying the flow rates of the ferrofluid in the range 5 μl/min–40 μl/min and the aqueous stream in the range 40 μl/min–150 μl/min. The conditions for achieving a stable interface in the coflow system are illustrated in the supplementary material, Sec. S.5. The interface location is varied by controlling the flow rate ratio of the aqueous and ferrofluid streams (see Fig. S.5b). Droplets of size ranging from 20 to 120 μm were generated, and the droplet migration toward the interface and coalescence with the aqueous stream was studied by varying the magnetophoretic force and the flow rate.

Figure 4(a) depicts experimental images showing time evolution of migration of an aqueous droplet of size 52 μm toward the ferrofluid-aqueous interface, with the ferrofluid and aqueous stream at flow rates 15 μl/min and 50 μl/min, respectively. The spacing between the center of the magnet and the channel center was 8.5 mm. Figure 4(b) (Multimedia view) shows the corresponding trajectory of the droplets. Now, let us illustrate the condition that needs to be satisfied in order to achieve magnetic-field based droplet coalescence. For a given width of the ferrofluid stream, the magnetophoretic force acting on the droplets should be strong enough so that the droplets migrate to the interface and overcome the disjoining pressure before exiting the magnetic field region. The location of the interface is characterized in terms of the width of the ferrofluid stream $w^* = (w_f/w)$. Figure 4(b) (Multimedia view) shows the coalescence and noncoalescence of droplets depending on the size, interface location, and magnetic field: droplets of size 30 μm with $w^* = 0.28$ and $(B \cdot \nabla B) = 18.55\ \mathrm{T^2/m}$ get coalesced, whereas droplets of size 30 μm with $w^* = 0.28$ and $(B \cdot \nabla B) = 1.25\ \mathrm{T^2/m}$ do not coalesce.

During migration and coalescence, the different forces acting on the droplets and the time scales involved are schematically represented in Fig. 4(c). The magnetocoalescence of an aqueous droplet occurs in two steps. First, due to the magnetophoretic force, the droplet migrates laterally from its original streamline to arrive at a location closer to the interface (at a small distance Δ from the interface) over a time scale τ_m. During this, there is a balance between the magnetic force and the drag force. Experimentally, the location at a distance Δ from the interface is identified as the location up to which the droplet velocity in the lateral direction varies within ±1% of the maximum lateral velocity of the droplet. In the case presented in Fig. 4(a) [and Fig. 4(b) (Multimedia view)—coalescence case], $\Delta \sim 1$ μm. Once the droplet arrives at a distance Δ from the interface, the lateral velocity of the droplet decreases abruptly to an infinitesimally small value [see Fig. 4(b) (Multimedia view)]. Second, beyond this location, the magnetic force is opposed by the hydrodynamic force arising from the drainage of the thin film of the

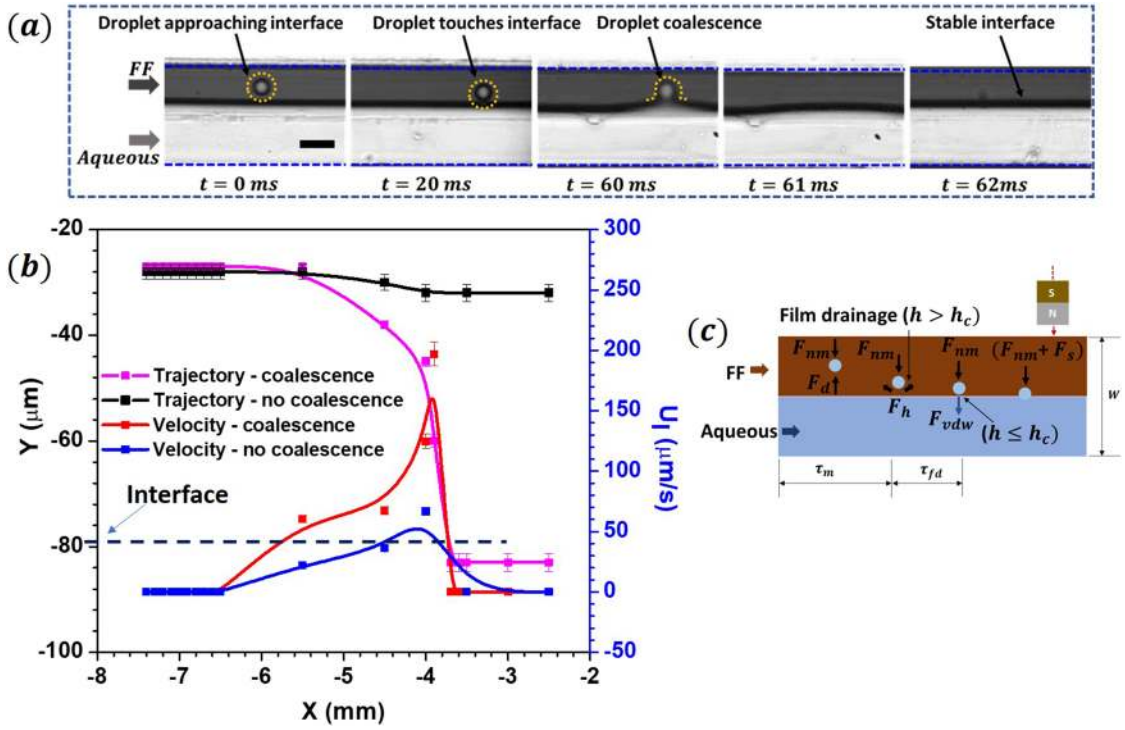

FIG. 4. (a) Experimental images showing the time evolution of migration of an aqueous droplet of size 52 μm toward the ferrofluid-aqueous stream interface, with the ferrofluid and aqueous streams at flow rates of 15 μl/min and 50 μl/min, respectively. The spacing between the center of the magnet and the channel center was 2 mm, and the scale bar represents 100 μm. (b) Coalescence and noncoalescence of droplets depending on the size, interface location, and magnetic field: droplets of size 30 μm with w^* = 0.28 and $(B \cdot \nabla B)$ = 18.55 T^2/m get coalesced, whereas droplets of size 30 μm with w^* = 0.28 and $(B \cdot \nabla B)$ = 1.25 T^2/m do not coalesce. (c) Different forces acting on the droplets and the time scales involved during migration and coalescence. Multimedia view: (b) https://doi.org/10.1063/1.5123533.2

ferrofluid between the aqueous droplet and the interface. The thin film drainage occurs over a time scale τ_{fd}, which is estimated as[45]

$$\tau_{fd} = \frac{\pi}{4}\left(\frac{h_i \mu_d r_f^4}{r_d h_c^2 F}\right), \tag{7}$$

where h_i is the initial film thickness, μ_d is the droplet viscosity, r_f is the film radius, r_d is the droplet radius, F is the applied force (i.e., magnetic force in the present case), and h_c is the critical film thickness below which spontaneous coalescence occurs due to the van der Waals interaction (~25 to 50 nm). An accurate estimation of the thin film drainage time scale τ_{fd} is very challenging due to the varied length scales involved in the thin film drainage process, namely, droplet radius (~100 μm), film radius r_f (~10 μm), and film thickness h_c (~50 nm). Taking r_f = 5 μm, the critical thickness as 50 nm, the droplet radius of 50 μm, and the magnetic force F_{nm} ~ 0.38 μN, the value of τ_{fd} calculated from the above equation is 0.23 s, which compares well with the experimental thin film drainage time of 0.28 s [for the case in Fig. 4(b) (Multimedia view)—coalescence]. Finally, when the thin-film thickness approaches ~25 nm, the force due to disjoining pressure (van der Waals force), which is attractive in the present case (since the Hamaker constant A_H is positive), gives rise to instant coalescence of the droplet with the aqueous stream. From experiments, we found that the coalescence time scale τ_{col} is of the order of 1.0 ms or less, which is negligible ($\tau_{col} \ll \tau_m$) compared to τ_m and τ_{fd} (that are of the order of 0.1–1.0 s).

Despite the above limitations for accurate theoretical estimation of τ_{fd}, from experiments, we find that the above two time scales τ_m and τ_{fd} are related as $\tau_{fd} = a\tau_m^{-0.33}$ (with a = 1, R^2 = 0.99), which indicates that if τ_m increases then τ_{fd} decreases and vice versa [see Fig. 5(a)]. This is attributed to the magnetic force distribution and the time evolution of droplet migration and coalescence shown in Fig. 5(b). Irrespective of the magnitude of the individual time scales, droplet coalescence always occurs at a position coinciding with the peak magnetic field located at the left edge of the magnet, where the magnetic force is the highest [see Fig. 5(b)]. If the magnetic time scale τ_m is smaller, a droplet comes in contact with the interface further upstream (from the coalescence point), and in that case, the film-drainage time scale τ_{fd} will be higher. Similarly, if the magnetophoretic time scale τ_m is higher, a droplet comes in contact with the interface further downstream (but ahead of the coalescence point), and in that case, the film-drainage time scale τ_{fd} will be lower.

The film-drainage phenomenon affecting the coalescence can be represented by a thin-film Reynolds number, Re_{fd}, which is the ratio of the film-drainage (viscous) time scale τ_{fd} and the advection scale τ_a, i.e., $Re_{fd} = (\tau_{fd}/\tau_a)$. Hence, the migration and coalescence behavior can be represented in terms of the ratio of the total

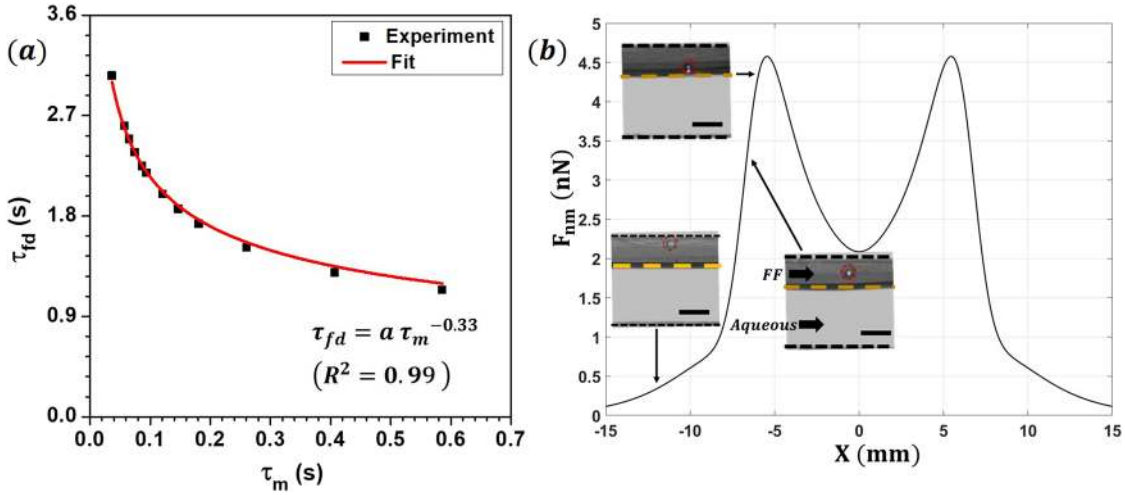

FIG. 5. (a) Interdependency of time scales τ_m and τ_{fd}: if τ_m increases, then τ_{fd} decreases and vice versa. (b) Variation in the magnetic force along the flow direction and images of the cross-stream migration and coalescence of droplets are shown in the inset.

migration time scale to the advection time scale as $\xi = (\tau_m + \tau_{fd})/\tau_a = (St^{-1} + Re_{fd})$. In Fig. 6, for a droplet of 20 μm diameter, flow rates of the ferrofluid and aqueous stream 10 μl/min and 80 μl/min, respectively, and magnetic field $(B \cdot \nabla B) = 18.55$ T^2/m, from experiments, the time taken by the droplet to reach from the nearby wall to the ferrofluid-aqueous interface is $\tau_m = 0.14$ s, while the time taken to drain the thin oil film present between the aqueous droplet and aqueous continuous phase is $\tau_{fd} = 1.86$ s. Thus, the total migration time scale is experimentally measured to be $(\tau_m + \tau_{fd}) = 2$ s. However, the advection time scale was calculated to be $\tau_a = 0.054$ s, which results in $\xi = 37.03$ for which coalescence is observed. For the same droplet size and magnetic field, with flow rates of the ferrofluid and aqueous stream 20 μl/min and 80 μl/min, respectively, the total migration time scale is measured to be $(\tau_m + \tau_{fd}) = 2.05$ s; on the contrary, the advection time scale is estimated to be $\tau_a = 0.027$ s; thus, coalescence is not observed at $\xi = 81$. The higher flow rate of the ferrofluid results in smaller advective time scale τ_a, which restricts the droplet coalescence.

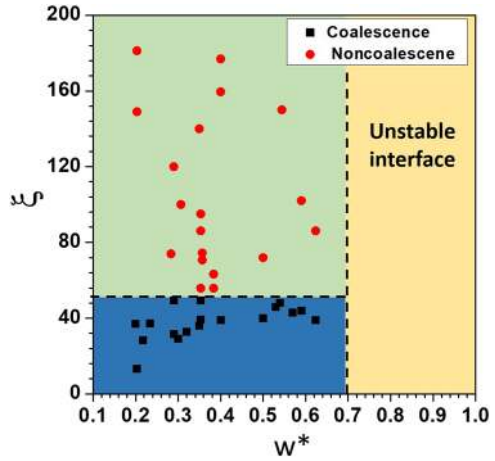

FIG. 6. The magnetophoretic coalescence and noncoalescence regimes are characterized based on the ratio of the width of the ferrofluid stream to that of the channel width (w^*) and the ratio of total migration time scale to the advection time scale ξ. Magnetocoalescence of droplets is observed for $w^* < 0.7$ (stable interface) and $\xi \leq 50$, and the boundaries demarcating the various regimes are identified by analyzing the experimental data.

Next, we performed experiments by varying the ferrofluid to the aqueous stream flow rate ratios, magnetic field, and droplet size and propose a general criterion for magnetocoalescence of droplets. The magnetophoretic coalescence and noncoalescence regimes are characterized based on two different parameters: the ratio of the width of the ferrofluid stream to that of the channel w^* and the ratio of total migration time scale and the film drainage time scale to the advection time scale ξ, which is depicted in Fig. 6. The various data points are obtained by performing a large set of experiments by changing various parameters—the flow rate of the continuous phase (oil based ferrofluid), droplet size, magnetic flux density, and its gradient. Based on the experimental results, the coalescence and noncoalescence regimes were identified as depicted in Fig. 6. As explained in Sec. S.4 in the supplementary material, for $w^* > 0.7$, the interface becomes unstable and the aqueous stream breaks into droplets, which is attributed to the excessive shear stress. For $w^* < 0.7$, a stable interface is established, and depending on the value of ξ, the coalescence or noncoalescence of droplets is observed. As observed, for $\xi \leq 50$, the coalescence of droplets is observed since the total migration time is much smaller than the advection time. On the other hand, for $\xi > 50$, the droplets do not get coalesced and continue to flow in the ferrofluid.

C. Extraction of microparticles from aqueous droplets

In this section, extraction of microparticles encapsulated in aqueous droplets into the coflowing aqueous stream is demonstrated. The materials and methods used for preparing the

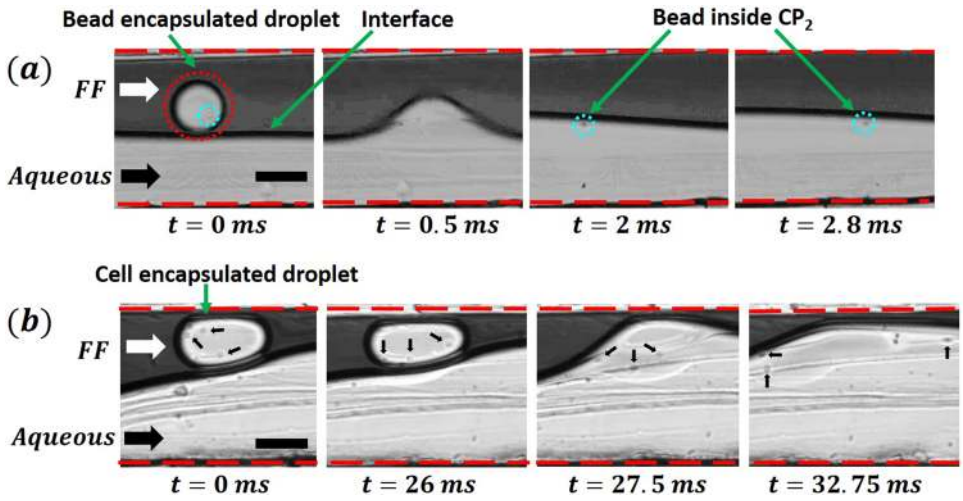

FIG. 7. Experimental images (bright field) showing the extraction of (a) a polystyrene microbead of size 10 μm from an aqueous droplet of size 67 μm flowing in an aqueous ferrofluid at a flow rate 15 μl/min with an aqueous stream at a flow rate 80 μl/min (w^* = 0.52) in the presence of a magnetic field ($B \cdot \nabla B$) = 18.55 T^2/m. (b) HeLa cells of size 40 μm from an aqueous droplet of size 120 μm flowing in an aqueous ferrofluid at a flow rate 10 μl/min with an aqueous stream at a flow rate 80 μl/min (w^* = 0.52) in the presence of a magnetic field ($B \cdot \nabla B$) = 18.55 T^2/m. Scale bar represents 100 μm.

microbeads and cell samples are detailed in Sec. III. The polystyrene microbead suspension is used as the discrete phase, and the oil based ferrofluid is used as the continuous phase. The corresponding flow rates of the microbead suspension and the ferrofluid at the T-junction were 1.0 μl/min and 15 μl/min to generate bead encapsulated droplets, respectively. DI water is used as the continuous phase and was infused at 80 μl/min. In the absence of the magnetic field, droplets with beads follow their own streamline without coalescing with the aqueous phase. Upon exposure to a magnetic field, due to the magnetophoretic force, the droplets undergo cross-stream migration toward the interface. At the interface, the interplay between the magnetophoretic force, the hydrodynamic force due to film-drainage, and the van der Waals attraction leads to droplet coalescence, and thus, extraction of the microbeads from the aqueous droplets into aqueous stream takes place. The extraction of microbeads is captured using a high-speed camera (FASTCAM SA5, Photron, Inc., UK) at 4000 fps (to capture the coalescence process). Experimental images showing the extraction of a microbead of size 10 μm from an aqueous droplet of size 67 μm in the presence of a magnetic field are shown in Fig. 7(a). Similarly, biological cells (HeLa) are encapsulated in PBS droplets with the oil based ferrofluid as the continuous phase. Using the same operating conditions used in the case of microbead extraction, the cells are extracted from the aqueous (PBS) drops into the aqueous stream. Experimental images showing the extraction of a HeLa cells from an aqueous droplet of size 120 μm in the presence of a magnetic field are shown in Fig. 7(b).

V. CONCLUSIONS

In summary, we reported the physics of cross-stream migration and the coalescence of aqueous liquid droplets flowing in an oil based ferrofluid with a coflowing aqueous stream upon exposure to a magnetic field. We found that the magnetophoretic migration phenomenon is governed by the advection (τ_a) and magnetophoretic (τ_m) time scales. Our results showed that the equilibrium cross-stream migration distance δ depends on the Strouhal number, $St = (\tau_a/\tau_m)$, as $\delta^* = 1.1\ St^{0.33}$ (with $R^2 = 0.97$), whereas the length L_δ required to attain equilibrium cross-stream migration depends on the St as $L_\delta{}^* = 5.3\,St^{-0.50}$ (with $R^2 = 0.90$). Our study revealed that the droplet-stream coalescence phenomenon is underpinned by the ratio of the sum of magnetophoretic (τ_m) and film-drainage time scales (τ_{fd}) and the advection time scale (τ_a), expressed in terms of the Strouhal number (St) and the film-drainage Reynolds number (Re_{fd}) as $\xi = (\tau_m + \tau_{fd})/\tau_a = (St^{-1} + Re_{fd})$. The results showed that τ_m and τ_{fd} are related as $\tau_{fd} = a\tau_m{}^{-0.33}$ (with $a = 1$, $R^2 = 0.99$). We studied the coalescence and noncoalescence regimes by varying the flow rates of the coflowing streams, droplet size, and magnetic field and found that droplet-stream coalescence is achieved for $\xi \leq 50$ and stream width ratio $w^* < 0.7$. We demonstrated the extraction of microparticles (beads and cells) from aqueous droplets to an aqueous stream. The proposed droplet coalescence technique based on the magnetophoretic force will find applications in biochemical assays.

SUPPLEMENTARY MATERIAL

See the supplementary material for (S.1) the device and experimental setup, (S.2) the variation of the magnetic flux density and equations used to estimate the force distribution using MATLAB, (S.3) the effect of the droplet size and flow rate on droplet trajectories, (S.4) the variation of lateral velocity of the droplet along the flow direction, and (S.5) conditions for achieving a stable interface and an effect of flow rate ratio on the interface location.

Supporting videos multimedia Figs. 2 and 4 show the cross-stream migration of droplets and coalescence and noncoalescence of droplets.

ACKNOWLEDGMENTS

We thank SERB, DST, India (Grant No. EMR/2014/001151) and I.I.T. Madras (Grant No. MEE/15-16/843/RFTP/ASHS) for providing the financial support which enabled this work. We also acknowledge CNNP, IIT Madras for supporting device fabrication.

NOMENCLATURE

τ_a	advection time scale
τ_m	magnetic time scale
δ^*	equilibrium cross-stream migration distance
$L_\delta{}^*$	length required to attain the equilibrium cross stream migration distance (δ^*)
St	Strouhal number
τ_{fd}	film drainage time scale
Re_{fd}	film drainage Reynolds' number
ξ	a ratio equal to $St^{-1} + Re_{fd}$
w^*	ferrofluid stream width ratio
F_l	noninertial lift force
F_{nm}	negative magnetophoretic force
F_d	viscous drag
F_h	hydrodynamic force due to the film drainage
h_c	critical film thickness
F_{vdw}	van der Waals force
τ_{col}	coalescence time scale

REFERENCES

[1]L. Wu, P. Chen, Y. Dong, X. Feng, and B. F. Liu, "Encapsulation of single cells on a microfluidic device integrating droplet generation with fluorescence-activated droplet sorting," Biomed. Microdevices **15**, 553 (2013).

[2]H. Song, D. L. Chen, and R. F. Ismagilov, "Reactions in droplets in microfluidic channels," Angew. Chem., Int. Ed. **45**, 7336 (2006).

[3]S. Dhiman, K. S. Jayaprakash, R. Iqbal, and A. K. Sen, "Self-transport and manipulation of aqueous droplets on oil-submerged diverging groove," Langmuir **34**, 12359 (2018).

[4]K. S. Khalil, S. R. Mahmoudi, N. Abu-Dheir, and K. K. Varanasi, "Active surfaces: Ferrofluid-impregnated surfaces for active manipulation of droplets," Appl. Phys. Lett. **105**, 041604 (2014).

[5]D. Jiang and S.-Y. Park, "Light-driven 3D droplet manipulation on flexible opto-electrowetting devices fabricated by a simple spin-coating method," Lab Chip **16**, 1831 (2016).

[6]C. G. Yang, Z. R. Xu, and J. H. Wang, "Manipulation of droplets in microfluidic systems," TrAC, Trends Anal. Chem. **29**, 141 (2010).

[7]K. S. Jayaprakash, U. Banerjee, and A. K. Sen, "Dynamics of aqueous droplets at the interface of coflowing immiscible oils in a microchannel," Langmuir **32**, 2136 (2016).

[8]X. Chen, C. Xue, L. Zhang, G. Hu, X. Jiang, and J. Sun, "Inertial migration of deformable droplets in a microchannel," Phys. Fluids **26**, 112003 (2014).

[9]A. A. S. Bhagat, S. S. Kuntaegowdanahalli, and I. Papautsky, "Continuous particle separation in spiral microchannels using dean flows and differential migration," Lab Chip **8**, 1906 (2008).

[10]R. Hajian and S. Hardt, "Formation and lateral migration of nanodroplets via solvent shifting in a microfluidic device," Microfluid. Nanofluid. **19**, 1281 (2015).

[11]A. Karbalaei, R. Kumar, and H. J. Cho, "Thermocapillarity in microfluidics—A review," Micromachines **7**, 13 (2016).

[12]S.-Y. Park, S. Kalim, C. Callahan, M. A. Teitell, and E. P. Y. Chiou, "A light-induced dielectrophoretic droplet manipulation platform," Lab Chip **9**, 3228 (2009).

[13]A. Srivastava, S. Karthick, K. S. Jayaprakash, and A. K. Sen, "Droplet demulsification using ultralow voltage-based electrocoalescence," Langmuir **34**, 1520 (2018).

[14]M. R. Hassan, J. Zhang, and C. Wang, "Deformation of a ferrofluid droplet in simple shear flows under uniform magnetic fields," Phys. Fluids **30**, 092002 (2018).

[15]C. Mandal, U. Banerjee, and A. K. Sen, "Transport of a sessile aqueous droplet over spikes of oil based ferrofluid in the presence of a magnetic field," Langmuir **35**, 8238 (2019).

[16]N. T. Nguyen, "Micro-magnetofluidics: Interactions between magnetism and fluid flow on the microscale," Microfluid. Nanofluid. **12**, 1 (2012).

[17]N. Vats, C. Wilhelm, P. E. Rautou, M. Poirier-Quinot, C. Péchoux, C. Devue, C. M. Boulanger, and F. Gazeau, "Magnetic tagging of cell-derived microparticles: New prospects for imaging and manipulation of these mediators of biological information," Nanomedicine **5**, 727 (2010).

[18]N. Pamme and A. Manz, "On-chip free-flow magnetophoresis: Continuous flow separation of magnetic particles and agglomerates," Anal. Chem. **76**, 7250 (2004).

[19]Y. Zhang and N.-T. Nguyen, "Magnetic digital microfluidics – a review," Lab Chip **17**, 994 (2017).

[20]L. H. P. Cunha, I. R. Siqueira, T. F. Oliveira, and H. D. Ceniceros, "Field-induced control of ferrofluid emulsion rheology and droplet break-up in shear flows," Phys. Fluids **30**, 122110 (2018).

[21]S. A. Peyman, E. Y. Kwan, O. Margarson, A. Iles, and N. Pamme, "Diamagnetic repulsion—A versatile tool for label-free particle handling in microfluidic devices," J. Chromatogr. A **1216**, 9055 (2009).

[22]A. Munaz, M. J. A. Shiddiky, and N. T. Nguyen, "Magnetophoretic separation of diamagnetic particles through parallel ferrofluid streams," Sens. Actuators, B **275**, 459 (2018).

[23]K. Zhang, Q. Liang, S. Ma, X. Mu, P. Hu, Y. Wang, and G. Luo, "On-chip manipulation of continuous picoliter-volume superparamagnetic droplets using a magnetic force," Lab Chip **9**, 2992 (2009).

[24]Y. J. Sung, J. Y. H. Kim, H. Il Choi, H. S. Kwak, and S. J. Sim, "Magnetophoretic sorting of microdroplets with different microalgal cell densities for rapid isolation of fast growing strains," Sci. Rep. **7**, 10390 (2017).

[25]R. E. Rosensweig, "Magnetic fluids," Annu. Rev. Fluid Mech. **19**, 437 (1987).

[26]U. Banerjee, A. Raj, and A. K. Sen, "Dynamics of aqueous ferrofluid droplets at coflowing liquid-liquid interface under a non-uniform magnetic field," Appl. Phys. Lett. **113**, 143702 (2018).

[27]J. Zhang, S. Yan, D. Yuan, Q. Zhao, S. H. Tan, N. T. Nguyen, and W. Li, "A novel viscoelastic-based ferrofluid for continuous sheathless microfluidic separation of nonmagnetic microparticles," Lab Chip **16**, 3947 (2016).

[28]X. Xuan, J. Zhu, and C. Church, "Particle focusing in microfluidic devices," Microfluid. Nanofluid. **9**, 1 (2010).

[29]W. Espulgar, Y. Yamaguchi, W. Aoki, D. Mita, M. Saito, J. K. Lee, and E. Tamiya, "Single cell trapping and cell-cell interaction monitoring of cardiomyocytes in a designed microfluidic chip," Sens. Actuators, B **207**, 43 (2015).

[30]S. Karthick and A. K. Sen, "Role of shear induced diffusion in acoustophoretic focusing of dense suspensions," Appl. Phys. Lett. **109**, 014101 (2016).

[31]D. Matsunaga, F. Meng, A. Zöttl, R. Golestanian, and J. M. Yeomans, "Focusing and sorting of ellipsoidal magnetic particles in microchannels," Phys. Rev. Lett. **119**, 198002 (2017).

[32]D. Di Carlo, D. Irimia, R. G. Tompkins, and M. Toner, "Continuous inertial focusing, ordering, and separation of particles in microchannels," Proc. Natl. Acad. Sci. U. S. A. **104**, 18892 (2007).

[33]D. Di Carlo, "Inertial microfluidics," Lab Chip **9**, 3038 (2009).

[34]T. Zhu, R. Cheng, and L. Mao, "Focusing microparticles in a microfluidic channel with ferrofluids," Microfluid. Nanofluid. **11**, 695 (2011).

[35]K. Zhang, Q. Liang, X. Ai, P. Hu, Y. Wang, and G. Luo, "On-demand microfluidic droplet manipulation using hydrophobic ferrofluid as a continuous-phase," Lab Chip **11**, 1271 (2011).

[36]R. Zhou and C. Wang, "Multiphase ferrofluid flows for micro-particle focusing and separation," Biomicrofluidics **10**, 034101 (2016).

[37]L. Mazutis and A. D. Griffiths, "Selective droplet coalescence using microfluidic systems," Lab Chip **12**, 1800 (2012).

[38]B. Xu, N.-T. Nguyen, and T. N. Wong, "Droplet coalescence in microfluidic systems," Micro Nanosyst. **3**, 131 (2011).

[39]T. Ichikawa, "Electrical demulsification of oil-in-water emulsion," Colloids Surf., A **302**, 581 (2007).

[40]V. B. Varma, A. Ray, Z. M. Wang, Z. P. Wang, and R. V. Ramanujan, "Droplet merging on a lab-on-a-chip platform by uniform magnetic fields," Sci. Rep. **6**, 37671 (2016).

[41]R. E. Rosensweig, R. Kaiser, and G. Miskolczy, "Viscosity of magnetic fluid in a magnetic field," J. Colloid Interface Sci. **29**, 680 (1964).

[42]D. Y. C. Chan, E. Klaseboer, and R. Manica, "Film drainage and coalescence between deformable drops and bubbles," Soft Matter **7**, 2235 (2011).
[43]V. Bergeron, "Forces and structure in thin liquid soap films," J. Phys.: Condens. Matter **11**, R215 (1999).
[44]E. Hemachandran, T. Laurell, and A. K. Sen, "Continuous droplet coalescence in a microchannel coflow using bulk acoustic waves," Phys. Rev. Appl. **10**, 044008 (2019).
[45]S. A. K. Jeelani and S. Hartland, "Effect of interfacial mobility on thin film drainage," J. Colloid Interface Sci. **164**, 296 (1994).
[46]C. Scherer and A. M. F. Neto, "Ferrofluids: Properties and applications," Braz. J. Phys. **35**, 718 (2005).
[47]D. Quéré, P.-G. De Gennes, and F. Brochard-Wyart, *Capillarity and Wetting Phenomena: Drops, Bubbles, Pearls, Waves* (Springer New York, New York, NY, 2013).
[48]P. Sajeesh, M. Doble, and A. K. Sen, "Hydrodynamic resistance and mobility of deformable objects in microfluidic channels," Biomicrofluidics **8**, 054112 (2014).
[49]K. S. Jayaprakash and A. K. Sen, "Droplet encapsulation of particles in different regimes and sorting of particle-encapsulating-droplets from empty droplets," Biomicrofluidics **13**, 034108 (2019).
[50]M. W. H. Ley and H. Bruus, "Continuum modeling of hydrodynamic particle–particle interactions in microfluidic high-concentration suspensions," Lab Chip **16**, 1178 (2016).